Russian Chemical Reviews **76** (12) 1107 – 1121 (2007) © 2007 Russian Academy of Sciences and Turpion Ltd

DOI 10.1070/RC2007v076n12ABEH003729

Tunnelling chemical reactions of hydrogen isotopes in quantum solids

V V Khmelenko, E P Bernard, S Vasiliev, D M Lee

Contents

I.	Introduction	1107
II.	Historical background	1107
III.	Studies of exchange tunnelling reactions of hydrogen isotopes in clusters forming impurity – helium solids	1109
IV.	Studies of H atoms in solid H_2 films at ultralow temperatures	1117
V.	Conclusions and future work	1120

Abstract. The kinetics of tunnelling reactions of hydrogen isotopes in solid molecular nanoclusters immersed in superfluid helium and the changes in the environment of the atoms during the course of these reactions are reviewed. Results of pulsed electron spin resonance show that a very large fraction (50% – 60%) of the stabilised atoms reside on the surfaces of the nanoclusters. The results of studies of the recombination and the exotic behaviour of hydrogen atoms in a solid molecular hydrogen matrix at ultralow temperatures (0.15 – 0.9 K) are also discussed. The bibliography includes 68 references.

I. Introduction

In this paper we review recent experimental and, briefly, theoretical studies of quantum chemical reactions of atomic hydrogen isotopes in solid molecular matrices at low and ultralow temperatures. We put our main emphasis on the experimental work utilising the magnetic resonance methods of electron spin resonance (ESR), nuclear magnetic resonance (NMR) and electron – nuclear double resonance (ENDOR).

We begin in Section II with a brief historical background of the research on the physical processes and chemical reactions which occur with atomic hydrogen isotopes trapped inside solid hydrogen and/or deuterium molecular matrices. In Section III, we present in more detail a description of the experimental procedure for the preparation of the nanoclusters in superfluid helium and the ESR methods (9 GHz continuous wave and pulsed spectrometers) used for these studies. We also discuss the studies of the kinetics of exchange tunnelling reactions of hydrogen isotopes at $T \sim 1.35$ K in nanoclusters of impurity – helium (Im – He) solids. The changes of the environment of the atoms during the course of these reactions and the trapping sites of atoms in nanoclusters are also reviewed. In Section IV we discuss the experimental techniques for studies of H atoms in solid H_2 films at ultralow (0.15 – 0.9 K) temperatures. We present the results of studies of the recombination and the exotic behaviour of H atoms in thin ($\sim$50 nm) H_2 films in this temperature range. Section V contains a summary, some conclusions and future prospects for investigations of tunnelling reactions of hydrogen isotopes.

V V Khmelenko Department of Physics, Cornell University, 14853 Ithaca, NY, USA. Fax (1-607) 255 64 28, tel. (1-607) 255 06 70, e-mail: khmel@ccmr.cornell.edu; Institute of Energy Problems for Chemical Physics (Branch), Russian Academy of Sciences, 142432 Chernogolovka, Moscow Region, Russian Federation. Fax (7-496) 680 35 73
E P Bernard, D M Lee Department of Physics, Cornell University, 14853 Ithaca, NY, USA. Fax (1-607) 255 64 28, tel. (1-607) 255 06 70, e-mail: epb22@cornell.edu (E P Bernard), tel. (1-607) 255 06 71, e-mail: dml20@cornell.edu (D M Lee)
S Vasiliev Department of Physics, University of Turku, 20014 Turku, Finland. Fax (358-2) 333 63 70, tel. (358-2) 333 59 39, e-mail: servas@utu.fi

Received 29 May 2007
Uspekhi Khimii **76** (12) 1185 – 1201 (2007)

II. Historical background

Studies of hydrogen atoms trapped in solid molecular matrices have a long history, starting in the mid-1950s. Jen *et al.*,[1,2] Wall *et al.*,[3] and Pietter *et al.*[4] performed the first investigations of H atoms in solid H_2. The main motivation for these studies was the achievement of high concentrations of stabilised H atoms for possible application as a rocket fuel. An advantage as compared to existing chemical fuels would be realised only if concentrations of H atoms in solid H_2 of order 7.5% could be achieved.[5] Various methods were employed for producing H atoms, such as electron and γ-ray bombardment of solid H_2, deposition of the products of electrical discharges in gaseous H_2 on cold surfaces, and the addition of low concentrations of radioactive T_2 to solid H_2. Electron spin resonance (ESR) was used to measure the H atom concentrations. It was found that the average concentrations of H atoms were very small (less than 0.01%). This fact made impossible any practical applications of $H - H_2$ solid mixtures. Moreover, the amounts of H atoms were found to decrease gradually due to their recombination:

$$H + H \longrightarrow H_2 .$$

A revival of interest in this system occurred only after three decades because it provided a unique opportunity to study the processes of quantum physical diffusion and quantum tunnelling reactions. The influence of isotopic effects on these processes could also be studied. According to the idea of Andreev and Lifshits,[6] at low enough temperatures, any impurity inside a crystal becomes delocalised and may freely move within certain energy bands in a fashion similar to the

conduction of electrons in metals. This proposal was followed by detailed theoretical studies by Kagan *et al.*[7] They suggested a phonon assisted mechanism for the physical diffusion of H atoms through the potential barriers in H_2 crystal lattices. The dependence of the recombination rate of H atoms in solid H_2 on temperature according to this mechanism was determined to be linear, as given by

$$k_H(T) = AT.$$

At the same time Ivliev *et al.*[8] experimentally studied the diffusion of H atoms in solid H_2. The main method for studying the process of quantum diffusion was to measure the rate of recombination of the atoms. However, before recombining, the atoms need to approach each other within a lattice constant. At close enough spacing between the atoms, they distort the lattice potential, and their motion may become severely impeded by the energy level mismatch between the neighbouring sites. Therefore, such 'recombinational' diffusion appears to be much slower than the actual spatial diffusion in an ideal crystal. The studies of the latter still remain an important and challenging task in this research field. It was found that at temperatures above 4.3 K the recombination rate of H atoms follows the Arrhenius law,

$$k_H(T) \sim \exp\left(-\frac{E_a}{kT}\right),$$

where $E_a \sim 103$ K and k is the Boltzmann constant. However, in the temperature range 1.3 – 4.2 K a linear dependence of k_H on temperature was observed. The latter result was explained by the quantum diffusion mechanism discussed by Kagan *et al.*[7] From the measurements of the concentration of H atoms in these experiments it was possible to calculate the absolute rate constants and the value of the coefficient A in the formula $k_H(T) = AT$, which was found to be equal to $(2 \pm 1) \times 10^{-24}$ cm^3 s^{-1} K^{-1}. These results suggested that the physical quantum diffusion of H atoms in solid H_2 was an important process leading to recombination. In contrast, the Nagoya group led by Miyazaki[9] and the Chernogolovka group led by Gordon[10] suggested that the dominant process for the migration of H atoms in solid H_2 is the tunnelling exchange chemical reaction:

$$H + H_2 \longrightarrow H_2 + H, \quad (1)$$

which provides a chemical diffusion mechanism for the motion of the H atoms from one trapping site to another. Matrix isolated H atoms are confined to potential wells in a molecular H_2 matrix. These wells are not infinitely deep so it is possible for the H atom to tunnel *via* chemical reactions (1) through the matrix. For substitutional sites, tunnelling would correspond to a change in position of the atom by one lattice spacing, so the position of the atom and the neighbouring molecule are interchanged. This process could be repeated many times, thus providing a mechanism for an atom to move through the matrix. The barrier for this reaction is known[11] to be 4600 K, which is significantly larger than that for the physical diffusion of H atoms in solid H_2 ($\sim$100 K). On the other hand the potential barrier for exchange tunnelling is significantly narrower. Takayanagi *et al.*[12] performed theoretical calculations of rate constants for exchange tunnelling reactions of hydrogen isotopes. The theoretical prediction gives a very fast rate constant for reaction (1). Additionally, recent measurements of the recombination rates at different pressures up to 13 MPa show the independence of k_H on pressure.[13] This important finding could not be explained by physical diffusion, which should be suppressed with increasing pressure, thus supporting the hypothesis of chemical exchange tunnelling of H atoms.

The exchange chemical reaction:

$$D + D_2 \longrightarrow D_2 + D \quad (2)$$

is expected to be much slower because of the larger mass. The experimental results obtained by studying D atom recombination decay are in good qualitative agreement with theoretical predictions by Takayanagi *et al.*[12] Experimental studies of D atoms in bulk D_2 solids were performed by Sharnoff and Pound,[14] Iskovskikh *et al.*[15] and Miyazaki *et al.*[16–18] Deuterium atoms in D_2 nanoclusters were studied by Gordon *et al.*[10,19] and Bernard *et al.*[20,21] Iskovskikh *et al.* found that thermally activated diffusion is responsible for recombination of atoms at temperatures higher than 7 K, but at lower temperatures the two-phonon quantum physical diffusion of D atoms was suggested.[15] The latter mechanism explained the temperature dependence obtained for the rate constant, $k_D \sim T^9$. In contrast, Miyazaki *et al.*[16,17] and Gordon *et al.*[10] considered that the migration of D atoms through D_2 crystals occurred due to the tunnelling exchange chemical reactions similar to the case of H atoms in solid H_2.

Two important tunnelling exchange reactions that have also been studied experimentally are:

$$D + H_2 \longrightarrow HD + H, \quad (3)$$

$$D + HD \longrightarrow D_2 + H. \quad (4)$$

Exchange tunnelling reactions between atoms and molecules of hydrogen isotopes in solid mixtures were discovered by Gordon *et al.*[10] during studies of the stabilisation of nanoclusters containing H and D atoms produced by injection of a gaseous mixture into superfluid ^{4}He (at $T \sim 1.8$ K) after it had passed through a radiofrequency (RF) discharge. They found a large enhancement of the concentration of hydrogen atoms in hydrogen – deuterium solid samples so obtained, as compared with the content of hydrogen atoms in the initial gas jets. For example, for a gas content ratio $[H_2]/[D_2]$ equal to unity, they observed only ESR signals from hydrogen atoms, indicating an absence of D atoms. Considering all possible exchange chemical reactions between atoms and molecules of hydrogen isotopes, they concluded that due to differences in the zero-point energies of H_2, HD and D_2 molecules, only reactions (1) – (4) and reactions

$$H + HD \longrightarrow HD + H, \quad (5)$$

$$D + HD \longrightarrow HD + D \quad (6)$$

can occur, leading to a depletion of D atoms and a growth in the H atom population. Reactions:

$$H + D_2 \longrightarrow HD + D, \quad (7)$$

$$H + HD \longrightarrow H_2 + D \quad (8)$$

are endothermic and cannot proceed at the temperature of experiment. As a result of reactions (1) – (6), which occur at these temperatures mainly by tunnelling, H atoms tend to migrate through the matrix until they are surrounded by a shell of deuterium molecules or they recombine with other H atoms.

A few month later, Ivliev *et al.*[22] in Moscow and Tsuruta *et al.*[9] in Nagoya, Japan, using different experimental approaches, studied the evolution of concentrations of hydrogen and deuterium atoms in solid molecular hydrogen – deuterium mixtures, providing direct confirmation of exchange tunnelling reactions at low temperatures. The Nagoya group performed comprehensive quantitative studies of atoms in solid molecular matrices of hydrogen isotopes. They studied the rates of different tunnelling reactions,[9,16–18,23] the influence of o-H_2 in solid H_2 on the rate constant for reactions of H atoms,[24–26] the temperature effect on the reaction of atoms[27] and the trapping sites of the atoms in molecular matrices.[28–32]

These results were summarised in the monograph edited by Miyazaki.[33]

Ivanov *et al.*[34] have modeled the temperature dependence of the rate constant for tunnelling reaction (4) in the solid phase. Their model describes the rate constant K at lowest temperatures by the formula

$$\ln k = \ln k_0 + C_4T^4 + C_5T^5 + C_6T^6 + C_8T^8.$$

The coefficients in this formula were obtained from comparison with the experimental measurements of rate constants in the temperature range 2.6–6.5 K by Miyazaki *et al.*[27] The formula predicted that at the lowest temperatures $\ln k$ would be almost independent of temperature. Further studies of this reaction in the solid phase at lower temperatures would be desirable.

The exchange reactions between atoms and molecules of hydrogen isotopes have also been studied in cross beam experiments in gas phase at room temperature. Zhang and Miller[35] performed theoretical calculations of the rate constants for these reactions and obtained very good agreement with the experimental results.

During the past five years, the kinetics of exchange tunnelling reactions have been studied at Cornell in samples created by the method that originated in Chernogolovka.[36,37] The gel-like solids created in superfluid helium are now known as impurity–helium solids or alternatively as impurity–helium condensates.[38,39] Impurity–helium solids are highly porous gel-like nanomaterials consisting of interconnecting clusters of impurities with a characteristic size 5−9 nm and an average density over the entire sample volume as low as 10^{20} atoms (molecules) cm^{-3}. Each cluster contains approximately 10^4 atoms and molecules. This means that the concentration of the clusters in the impurity–helium solids is of order 10^{16} cm^{-3}. Tunnelling exchange reactions between atoms and molecules of hydrogen isotopes could then be investigated in the collection of nanoclusters and the results could be compared with those obtained earlier in bulk solids. Reactions among chemically active atoms and molecules within nanoclusters are predicted to be more efficient and selective than analogous reactions in bulk material.[40]

Although most studies of H atoms in solid H_2 were performed at temperatures above 1 K, Webeler[41] studied the recombination heating in solid H_2 containing 0.03% radioactive T_2 in the temperature range 0.16 K $\leqslant T \leqslant$ 0.8 K. The β-decay led to the dissociation of H_2 molecules, thus providing a population of H atoms. Results show an increase of H atom concentration with time, followed by spontaneous decay. Lowering the temperature led to an increase in the energy release from the recombination of H atoms during spontaneous decay. The first studies of recombination rates of H atoms in solid H_2 in the temperature range 0.15–0.9 K were performed very recently by Ahokas *et al.*[42] A high-field ESR spectrometer,[43] in combination with a $^3He-^4He$ dilution refrigerator cryostat, was employed in these investigations.

III. Studies of exchange tunnelling reactions of hydrogen isotopes in clusters forming impurity–helium solids

1. A setup for studies of tunnelling reactions in nanoclusters

The experimental setup for investigating exchange tunnelling chemical reactions in nanoclusters at low temperatures at Cornell University is described in more detail elsewhere.[44] The experiments were performed in a specially designed Janis cryostat with a variable temperature insert (VTI), which is a thermally insulated chamber, separated from the main 4 K helium bath. A needle valve connects the main helium bath of the cryostat to the VTI. Continuously pumping the VTI while supplying helium from the main bath permits long-term investigations of impurity–helium solids well below the lambda temperature (2.17 K) of liquid helium. The lower part of the cryostat was placed between the pole pieces of a homogeneous Varian electromagnet for CW and pulsed ESR investigations. Impurity–helium solids with stabilised H and D atoms for ESR investigations were prepared *in situ* in the Janis cryostat. The homemade insert for formation and investigation of atoms contained in Im–He solids is shown in Fig. 1. For sample preparation, a gas mixture of H_2 and/or D_2 and He was transported from a room temperature gas handling system to the cryogenic region. To provide H and D atoms *via* dissociation of the gas molecules, high-power radio-frequency ($f \sim 50$ MHz, $P \sim 70$ W) was applied to electrodes around the quartz capillary carrying the mixed gases. The resulting jet of helium gas with a small fraction (1%–4%) of impurity atoms and molecules emerging from the quartz capillary was directed onto the surface of superfluid ^4He

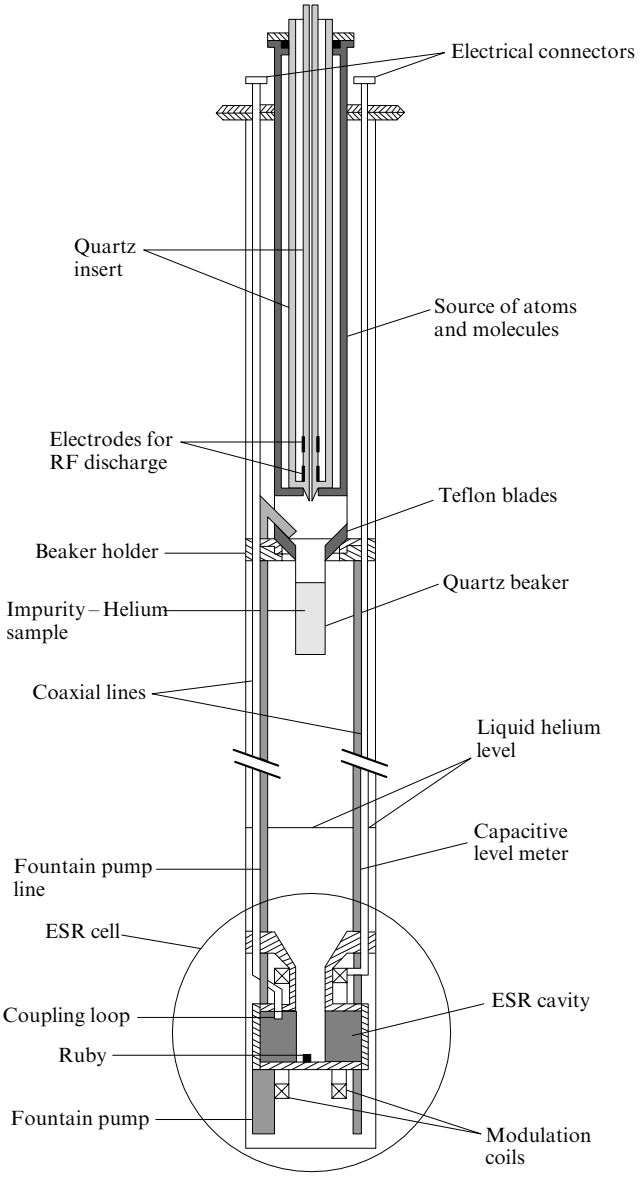


Figure 1. Low temperature insert used in the ESR investigation of Im–He solids.[44] The quartz beaker is lowered into ESR resonant cavity for measurements after sample preparation.

contained in a small beaker suspended above the VTI helium bath. The addition of helium gas increased the efficiency of dissociations of impurity molecules in the discharge due to interactions between the impurity and metastable He atoms and also retarded agglomeration of impurity atoms and molecules in the gas jet. The jet penetrated the surface of the liquid helium and a macroscopic snow-like translucent material was created. This material fell down through the liquid ^{4}He to form a porous solid at the bottom of the beaker. A fountain pump connected to the bottom of the helium bath in the VTI maintained a constant liquid helium level in the beaker. The temperature during sample preparation was 1.5 K. At the top of the beaker was a funnel that caught the sample as it condensed below the helium surface, which was 2 cm below the end of the quartz capillary. A set of teflon blades scraped the sample from the funnel while the beaker was rotated so that the sample could fall to the bottom of the cylindrical part of the beaker. A jet with a flux of $\sim 5 \times 10^{19}$ atoms and molecules per second yielded $\sim 0.3-0.4$ cm^3 of sample in 10 minutes.

In independent X-ray scattering studies of the D_2-He and $D_2-Ne-He$ samples, it was shown that these samples consisted of nanoclusters of D_2 molecules, each surrounded by thin layers of solid helium.[20,21] The typical deuterium cluster size is estimated to be $\sim 5-9$ nm. These nanoclusters assemble into a porous gel-like structure. From the comparison of the intensity of the D_2 cluster peak with the intensity of the scattering from liquid helium, the molecular deuterium densities in these samples were found to be of order 10^{20} cm^{-3}. It was difficult to carry out structural studies of H_2-He solids because solid hydrogen tends to float to the surface of the collection beaker filled with superfluid helium. Actual studies of hydrogen clusters in this research were performed with $H_2-Ne-He$ solids prepared with a mixture of hydrogen and neon make-up gas. The heavier neon clusters allowed the mixture to accumulate in the sample cell. An X-ray investigation of similar $D_2-Ne-He$ solids provided evidence that neon and deuterium existed in separate clusters in the sample. The result justifies the assumption that H_2 and Ne mainly occurred in separate nanoclusters in these experiments.

After sample preparation, the beaker containing the sample was lowered into the ESR cavity, which was situated at the bottom of the cryostat in the homogeneous field region of the Varian 7800 electromagnet. The volume occupied by the sample inside the cavity was 0.35 cm^3. The homemade cylindrical cavity was operated in the TE_{011} mode. The cavity has an axial hole to provide access for the sample to be introduced. Two different inserts were used in the experiments, one for detection of CW ESR signals by an X-band homodyne spectrometer and the other for detection of electron spin echo signals by a pulsed X-band homodyne spectrometer. Only the microwave cavities were different in these inserts. A high quality factor cavity ($Q \sim 3000$) was used in the CW ESR experiments, while in the pulsed ESR experiments a low quality factor cavity ($Q \sim 700$) was employed to avoid a long cavity ring-down time. CW and pulsed ESR signals were obtained for samples immersed in liquid helium at temperatures ~ 1.35 K. CW ESR signals were recorded by using a continuous wave reflection homodyne spectrometer (Varian E-4) operating near 9.1 GHz. Derivatives of the ESR absorption lines were detected at ~ 0.32 T by lock-in amplification using an additional small amplitude modulation field oscillating at 100 kHz. Atomic concentrations were measured by comparing the intensity of the atomic signals with the intensity of a signal from a small ruby crystal that was used as a secondary standard. The ruby crystal was attached permanently to the bottom of the microwave cavity. The calibration of the absolute value of the number of spins in the ruby crystal was made by using a standard organic diphenyl-picrylhydrazyl (DPPH) sample with a known number $\sim 2.4 \times 10^{17}$ of spins. The measurements were carried out at $T = 1.35$ K. A nuclear magnetic resonance (NMR) magnetometer was used for precise measurements of the applied magnetic field.

For pulsed ESR studies of atoms in Im – He solids, a special homodyne detection spectrometer was designed.[45] The spectrometer operates in the X-band region with a microwave frequency of 8930 MHz. Figure 2 shows a simplified block scheme of the pulsed ESR spectrometer. A 12-channel programmable pulse generator, operating at a 125-MHz clock frequency, provides logic signals to the P – I – N diode switch, bi-phase modulator, oscilloscope trigger and traveling wave tube (TWT) grid modulator. Microwaves from the tunable oscillator are amplified and split into pulse and reference paths. The pulses are amplified by a 1 kW, 50 dB TWT amplifier operating in the saturated regime. The amplified pulses pass through a circulator before transitioning to a 20 cm length of stainless steel coax at the entrance to the cryostat. (A similar arrangement was used in the CW spectrometer). This prevents excessive heat conduction into the cryostat. A low loss coax traverses the remaining 107 cm to the resonant cavity at the bottom of the cryostat, which is situated between the poles of the Varian electromagnet. Echo signals return through the same cabling to the circulator, which routes them to a low noise amplifier (LNA) that is protected by a diode limiter from the powerful microwave pulses. After amplification, a quadrature mixer provides homodyne detection by referencing the echo signals to the microwave oscillator. The resulting in-phase and quadrature signals are sampled by a digital oscilloscope and transferred *via* GPIB to a computer. The spectrometer design differs from other machines used to acquire electron spin echo data at cryogenic temperatures in three significant ways.[46] First, space constraints in our cryostat require the use of a coax rather than a waveguide connection to our cavity-type resonator. Second, our resonant cavity is a modified CW ESR

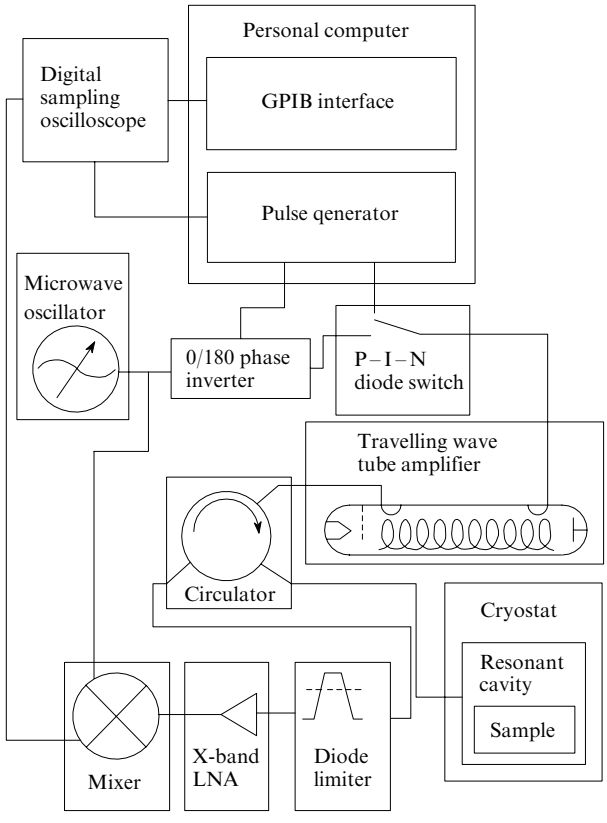


Figure 2. Block diagram of pulsed ESR spectrometer.

quartz-filled cavity designed to admit a funnel containing Im – He solid samples. To facilitate broadband excitation by short pulses, a chromium coated quartz ring is bonded with epoxy to thin fingers protruding from a brass pedestal. Adjusting the pedestal position then adjusts the Q factor of the cavity; we have found a Q of ~ 700 to be effective for detecting electron spin echo envelope modulation (ESEEM) due to deuterium nuclei. Further details of this method will be provided in a later section. For this apparatus, a 90° pulse has duration 40 ns. Finally, the spectrometer output is sampled by a sampling oscilloscope, not a boxcar integrator. Integrating a narrow section of the echo peak recovers standard boxcar ESEEM data. Alternatively, for two-pulse ESEEM experiments the echo can be sectioned in time and the phase correction algorithm of Astashkin *et al.* applied.[47] This corrects for the fact that the phase of the modulation harmonics varies within each echo, and therefore allows the entire echo to contribute to the signal, thus improving the signal/noise ratio.

2. CW ESR studies of tunnelling exchange reactions of hydrogen isotopes in clusters forming impurity – helium solids

The Im – He solids formed by injection of hydrogen isotopes into He II are of special interest due to their potential to manifest various quantum phenomena. The observation of tunnelling exchange chemical reactions between atoms and molecules of hydrogen isotopes at low temperatures in Im – He solids represents an important example of such a quantum phenomenon. Investigations of tunnelling reactions in Im – He solids were first performed by the Chernogolovka group.[10, 19] By using the CW ESR method, they studied the efficiency of the stabilisation of hydrogen and deuterium atoms in Im – He solids using hydrogen – neon – helium, deuterium – helium, or hydrogen – deuterium – helium gas mixtures. In contrast with earlier work, it was found that maximum local concentrations of H and D atoms as high as 1% could be easily achieved in Im – He solids. However, they were not able to study the time evolution of the concentration of stabilised atoms.

Recently, studies of the kinetics of tunnelling exchange reactions between atoms and molecules of hydrogen isotopes in nanoclusters have been performed by the Cornell group.[44, 48 – 51] The X-band CW ESR method was used in these studies. This method allows a determination of the time dependence of the hydrogen and deuterium atom concentrations during the tunnelling exchange reaction and it also provides information concerning changes in the environment of these atoms as the reactions proceed.

Initially the kinetics of tunnelling reactions were studied in each of the two pure hydrogen isotopes. The main features of the atomic hydrogen and atomic deuterium spectra recorded from a sample with initial gas mixtures in the ratios $H_2 : Ne : He = 1 : 4 : 100$ and $D_2 : He = 1 : 20$ are shown in Fig. 3. The hydrogen ESR lines are accompanied by two satellite lines, one on either side of the main line. The satellite lines are assigned to forbidden transitions involving an electron spin flip and a simultaneous spin flip of a proton on a neighbouring ortho-hydrogen molecule. Each of the ESR signals of H atoms was fitted with a sum of three Gaussians (one central line plus two symmetric satellites). From these fits the ratio of the intensities of the satellite and main lines is found to be 0.2. The splittings observed between the main and satellite lines (4.5 ± 0.1 G) are consistent with a proton spin flip in the 3 kG field. Because of the small nuclear magnetic moment of the deuteron, the corresponding splitting for electron spin – deuteron spin interactions is only 0.7 G. This is unobservable in these experiments because the ESR linewidths of the main lines are about 2 G and thus the small satellite lines are hidden by the broad main lines.

In the mixed samples, which contain both H and D atoms, the observation of satellite lines provides strong evidence that a

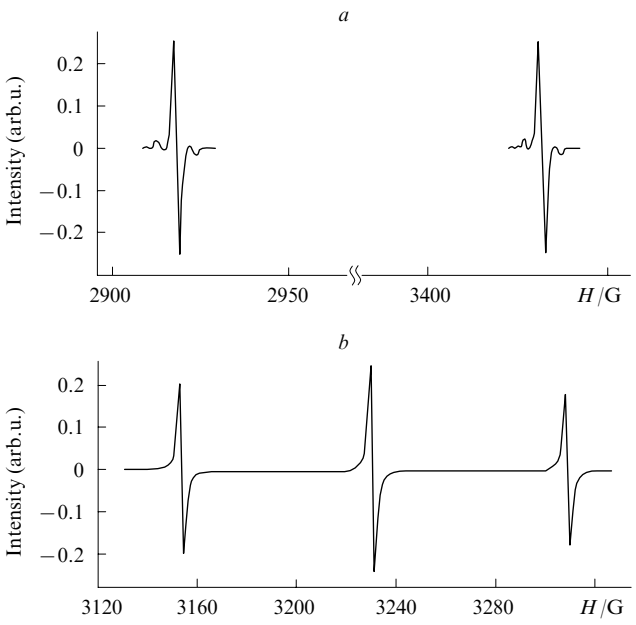


Figure 3. CW ESR derivative signals of atomic hydrogen in Im – He solid prepared from $H_2 : Ne : He = 1 : 4 : 100$ gas mixture (*a*) and of atomic deuterium in Im – He solid prepared from a $D_2 : He = 1 : 20$ gas mixture (*b*). ESR spectra were obtained at $T = 1.35$ K.

large fraction of the hydrogen and deuterium atoms are found in clusters of molecular hydrogen and/or molecular HD. In other words, they are not isolated as individual atoms separated by layers of solid helium. Therefore the solid samples provide a unique opportunity to carry out quantitative studies of the kinetics of tunnelling reactions of hydrogen isotopes in nanoclusters. The results of such experiments can then be compared with analogous studies performed in bulk solid mixtures of hydrogen isotopes. Different behaviour can be expected as a result of the large surface areas of the clusters.

According to Trammel *et al.*[52] the intensity ratio between the satellite lines and their respective main lines is proportional to the number of protons surrounding a stabilised atom and is strongly dependent on their positions:

$$\frac{I_{\mathrm{sat}}}{I_{\mathrm{main}}} = \frac{3}{20}\left(g_{\mathrm{e}}\frac{\beta_{\mathrm{e}}}{H_0}\right)^2 \langle r^{-6}\rangle N. \tag{9}$$

In the above equation g_e is the electron g factor, β_e is the Bohr magneton, H_0 is the applied magnetic field, r is the distance from an atom to a proton belonging to a neighbouring molecule, and N is the number of these protons. If a reasonable assumption can be made for the number of protons in molecules surrounding the atom, then the average distance between the atom and molecules can be found. Moreover, from the time dependence of this ratio during the course of the chemical reactions, it is possible to obtain the changes in the number of ortho-hydrogen molecules surrounding the atoms.

The time dependence at $T = 1.35$ K of the average concentration of H atoms in a $H - H_2 - Ne - He$ sample and that of D atoms in a $D - D_2 - He$ sample are displayed in Fig. 4. The addition of neon was required in the former sample because, unlike the $D_2 - He$ sample, the $H_2 - He$ solid does not sink to the bottom of the cell, due to its small density. As mentioned earlier, the tunnelling exchange reactions drive the migration of isolated atoms. The relatively fast migration of a hydrogen atom due to the tunnelling reaction (1) leads to recombination with another H atom ($H + H \rightarrow H_2$), and thus explains the

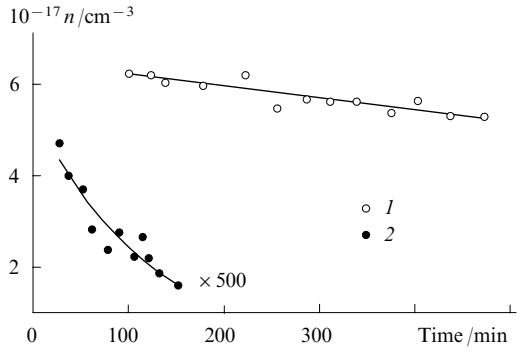


Figure 4. Time dependence of concentrations of atomic deuterium prepared from a D_2 : He = 1 : 20 gas mixture (*1*) and atomic hydrogen prepared from H_2 : Ne : He = 1 : 4 : 100 gas mixture (*2*) in Im – He solids stored at $T = 1.35$ K.[49]

rapid decay of the number of hydrogen atoms in the sample at $T = 1.35$ K.

The equation

$$\frac{dn}{dt} = -2\,k_H(T)n^2. \tag{10}$$

describes the decrease of the concentration of H atoms (n) with time (t) when the temperature of the sample is kept constant.[15] The experimental dependence of the variable $1/n$ on t should thus be linear, with the slope equal to $2\,k_H(T)$. The characteristic time (the half life) for the concentration to drop by 50% is

$$\tau_{1/2} = \left[2\,k_H(T)n_{H,\,loc}\right]^{-1}, \tag{11}$$

where $n_{H,\,loc}$ is the initial local concentration of H atoms. The average concentration of H atoms at the beginning of the measurements is $n_{H,\,av} = 10^{15}$ cm^{-3} according to Fig. 4. As indicated earlier the H_2 clusters and Ne clusters form separately. We shall make the reasonable assumption that the density of H_2 molecules in the H – H_2 – Ne – He samples is roughly similar to the density of D_2 in D_2 – He samples,[21] which is equal to $\sim 10^{20}$ cm^{-3}. This is more than two orders of magnitude lower than the density of the solid molecular hydrogen, which is equal to 2.4×10^{22} cm^{-3}. This means that the local concentration of H atoms in the clusters constituting the sample is two orders magnitude larger than the average concentration, giving $n_{H,\,loc} = 10^{17}$ cm^{-3}. The decay time of H atoms, $\tau_{1/2}$, shown in Fig. 4 is 150 ± 20 min. From Eqn (11), the rate constant for recombination of H atoms in solid H_2 was found to be $k_H(1.35) = 5.5 \times 10^{-22}$ cm^3 s^{-1}. This value is much larger than those obtained in bulk H_2 solids by the Nagoya group,[18] $k_H(1.9-4.2) = (4.4-5.9) \times 10^{-23}$ cm^3 s^{-1}, and the Moscow group,[8,15] $k_H(1.35) = 2.7 \times 10^{-24}$ cm^3 s^{-1}. This result may be due to a higher mobility of H atoms on the surfaces of the clusters or due to an inhomogeneous distribution of H atoms within the clusters.

The significantly slower decay of D atoms is attributed to the much slower migration of deuterium atoms through molecular deuterium due to the reaction (2). The same Eqn (10) describes the decrease of the concentration of D atoms with time. The initial local concentration of D atoms, $n_{D,\,loc}$, is equal to 6.25×10^{19} cm^{-3} and the characteristic decay time of D atoms is 2500 ± 500 min. From the relation

$$k_D = \frac{1}{2}\tau_{1/2}\,n_{D,\,loc},$$

it is found that

$$k_D(1.35\,\text{K}) = 5 \times 10^{-26}\ \text{cm}^3\ \text{s}^{-1}.$$

This value is in qualitative agreement with value $k_D(4.2) = 4 \times 10^{-26}$ cm^3 s^{-1}, obtained by Iskovskikh *et al.*[15] in solid D_2 at $T = 4.2$ K, but significantly larger than value $k_D = 3.3 \times 10^{-27}$ cm^3 s^{-1} obtained by Miyazaki *et al.*[17]

A completely different behaviour of hydrogen and deuterium atoms was observed in impurity – helium solids containing hydrogen and deuterium atoms along with hydrogen and deuterium molecules.[49] The main features of atomic hydrogen and deuterium spectra recorded from a sample with an initial gas mixture in the ratio H_2 : D_2 : He = 1 : 4 : 100 are shown in Fig. 5. Both the deuterium and the hydrogen ESR lines are

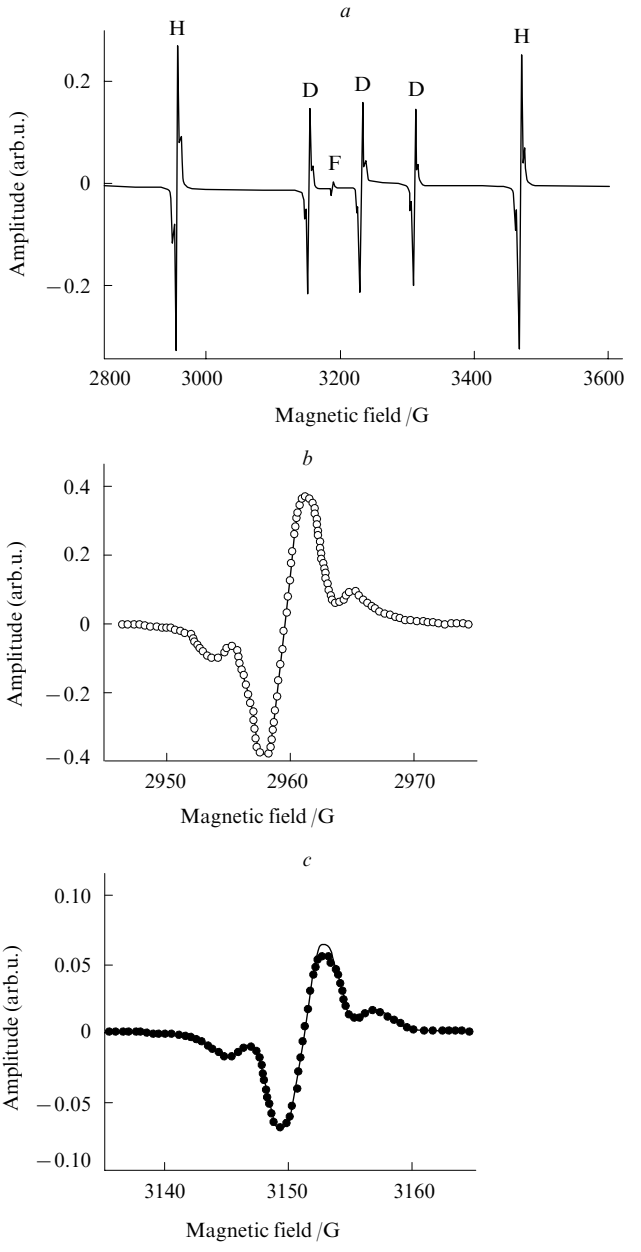


Figure 5. CW ESR derivative signal from Im – He sample prepared from gas mixture H_2 : D_2 : He = 1 : 4 : 100 (*a*). 'H' marks the allowed ESR transitions between the hyperfine levels of atomic H; 'D' indicates the hyperfine transitions of atomic D, and 'F' indicates the forbidden ESR transition of H atoms. Typical derivative signals for low field hyperfine line of hydrogen atoms (*b*) and deuterium atoms (*c*) show, at an expanded scale, both the allowed and the accompanying satellite lines. The lines in figures (*b* and *c*) represent simulations of the signals as the sum of three Gaussians.[49]

accompanied by two satellite lines symmetrically positioned about the main line. The satellite lines are assigned to forbidden transitions involving an electron spin flip and a simultaneous spin flip of a proton on a neighbouring HD or on an ortho-hydrogen molecule. The forbidden transition associated with the hyperfine levels of H atoms is also shown.

A large number of different initial gas mixtures were used for preparation of H_2-D_2-He solids.[44, 49] Immediately after preparation of all Im–He solids, a large enhancement of the H atom concentration relative to that of D atoms was observed, as compared to the ratio of H_2 to D_2 in the original gas mixtures. The fraction of H and D atoms as a function of the relative H_2 concentration in the condensed H_2-D_2 gas mixtures is shown in Fig. 6. The enhancement of the H atom concentrations at the earliest stage of sample preparation is attributed to the fast exchange tunnelling reaction (3), which leads to a large reduction in the number of D atoms and a corresponding increase in the number of H atoms with a time constant of order 1 min. During this reaction, most of the H_2 molecules that have neighbouring D atoms in the sample are converted into HD molecules. The rate constant for this reaction is calculated theoretically to be 3.56×10^{-25} cm^3 s^{-1} (Ref. 12). Recently, this tunnelling reaction was studied experimentally by Kumada [53] in bulk $HD-D_2$ and D_2-H_2 solid mixtures in the temperature range between 4 and 8 K. The reactions were initiated by UV photolysis of DI molecules doped in these solids for 30 s, followed by measuring the time variation of the ESR intensities of H and D atoms. The ESR intensity of D atoms produced by photolysis decreases but that of H atoms increases with time. The variation of the concentrations of the D and H atoms with time can be described in terms of a fast and a slow processes. The fast process, which was essentially complete within 300 s after photolysis, is assigned to the reaction (3). The rate constant for this reaction was determined to be $(2.9\pm0.3)\times10^{-25}$ cm^3 s^{-1} in solid $HD-H_2$ and $(5.0\pm1.1)\times10^{-25}$ cm^3 s^{-1} in solid D_2-H_2 mixtures at $T = 4.1$ K, which is very close to the theoretical calculations by Takayanagi *et al.*[12] These results provide very strong evidence favouring the role of tunnelling exchange reactions in the solid hydrogen isotopes.

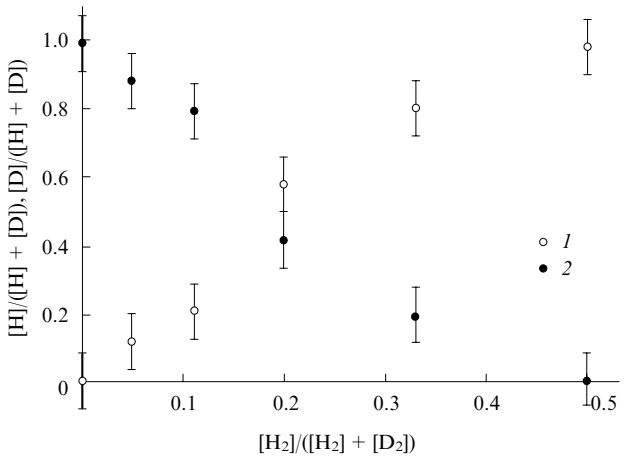


Figure 6. The dependence of the fractional concentrations of H (*1*) and D (*2*) atoms in the $HD-D_2-He$ samples as a function of H_2 content in the H_2-D_2 gas mixtures used for sample preparation.
For each point the concentrations were determined just after sample preparation.

For the case of Im–He solids, the time dependence of the concentration of H and D atoms on a longer time scale (2–40 h) showed a further increase in the concentration of H atoms. The simultaneous presence of deuterium and hydrogen molecules in the make up gas allows us to form impurity helium solids containing hydrogen atoms and deuterium atoms as well as hydrogen, deuterium, and hydrogen deuteride molecules. In Fig. 7 *a–c* we show the results obtained at Cornell, which dramatically illustrate the time dependence of the hydrogen and deuterium atom concentrations for different initial make-up gas mixtures.[49] In spite of the higher concentration of D_2 compared with that of H_2 in the sample produced from the initial gaseous mixture $H_2:D_2:He = 1:2:60$, the concentration of deuterium atoms is about two orders of magnitude smaller than the hydrogen atom concentration and it decays more rapidly (Fig. 7 *a*). These results are in sharp contrast to the Cornell studies of $H_2-Ne-He$ impurity solids, with no deuterium present, in which the decay of hydrogen atoms due to recombination was much more rapid. This can be explained by the presence of many D_2 and HD molecules in the sample, which lead to anomalously slow diffusion of the H atoms through the clusters, and by the partial replenishment of hydrogen atoms through the chemical reactions (3) and (4).

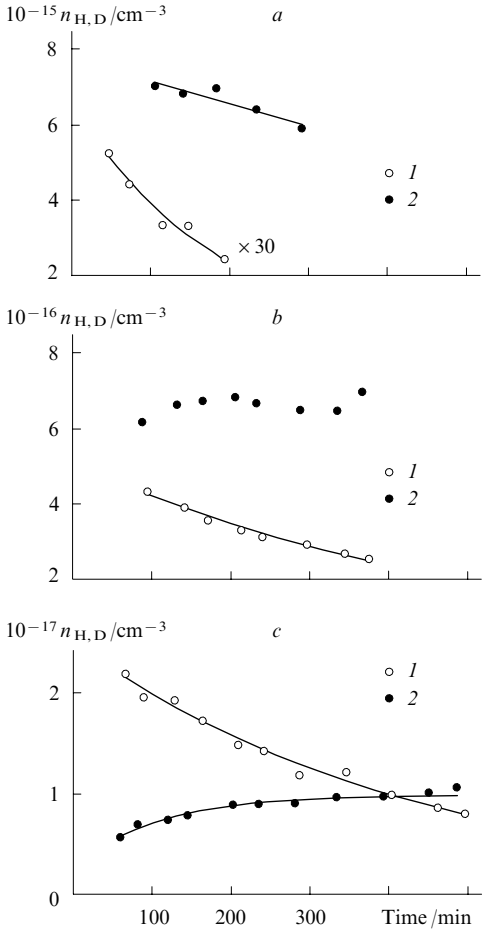


Figure 7. Time dependence of concentrations of atomic deuterium (*1*) and atomic hydrogen (*2*) in different Im–He solids at $T = 1.35$ K.[49]
$H_2:D_2:He$ mixture: 1 : 2 : 60 (*a*), 1 : 4 : 100 (*b*), 1 : 8 : 180 (*c*).

Furthermore, these reactions also explain the faster decrease of the deuterium atom concentration as compared with that in the $D-D_2-He$ sample (see Fig. 4). In Fig. 7 *b* the population of hydrogen atoms remains almost constant, meaning that the production is almost in balance with recombinational decay in the sample produced from an $H_2:D_2:He = 1:4:100$ mixture. In Fig. 7 *c* the population of hydrogen

atoms actually shows an increase that is driven by the chemical reactions as time evolves. The large initial supply of deuterium molecules in the gas mixture $H_2 : D_2 :$ He = 1 : 8 : 180 means that a copious supply of deuterium atoms is available in the sample, leading to a higher production of hydrogen atoms.

The exchange tunnelling reactions can be used to produce very large concentrations of atomic hydrogen in these mixed solids. In the Cornell studies samples obtained from a variety of initial gas mixtures have been investigated in order to determine the one which yields the highest hydrogen atom concentration.[44] The experimental plot shown in Fig. 8 gives the H and D average concentrations after a storage time $\sim$ 500 min following initial sample preparation. The largest concentration, of order $(7.5 \pm 3.0) \times 10^{17}$ cm^{-3}, was obtained by using the gas mixture $H_2 : D_2$: He = 1 : 4 : 100.

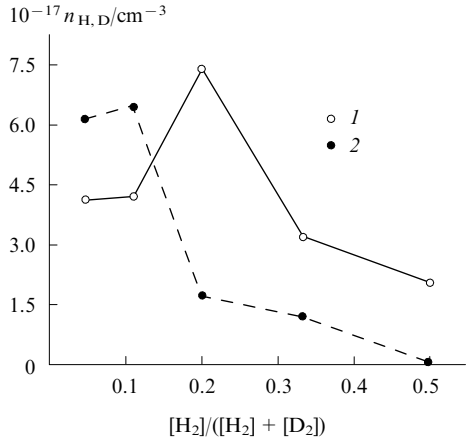


Figure 8. The dependence of the average concentrations of H atoms (*1*) and D atoms (*2*) in Im–He solids on the fraction of hydrogen gas in the make up gas mixture.[44]
For each point the concentrations were determined after a waiting period of 500 minutes following sample collection.

The very long term stability of the sample obtained from this gas mixture at a temperature of $T = 1.35$ K has also been studied in these investigations.[51] The time dependence of the logarithm of the average concentrations of H and D atoms in the sample produced from an initial gas mixture $H_2 : D_2$: He = 1 : 4 : 100 is displayed in Fig. 9. The concentration of H atoms remained constant throughout the 40-h experiment. During the same period of time, the concentration of D atoms decreased from its initial value of 10^{17} cm^{-3} by 2.5 orders of magnitude. The reaction (4) continued to eliminate D atoms and generate H atoms in the HD–D_2–He solid during the long-term experiment. From the decay rate of the D atoms, one can estimate a rate constant, k_{D-HD}, for this reaction from the equation

$$\frac{d[D]}{dt} = -k_{D-HD}[HD][D].$$

The decay time of D atoms was determined from the slope of the line presented in Fig. 9; $k_{D-HD} = 2.9 \times 10^4$ s. Assuming the impurity cluster density is close to that of solid D_2, one finds an initial HD concentration equal to 9.3×10^{21} cm^{-3} and a rate constant $k_{D-HD} = 3.6 \times 10^{-27}$ cm^3 s^{-1}, which agrees with the value found by Kumada *et al.*[27] in bulk samples.

The time dependence of the ratio of the satellite line to the main line for hydrogen and deuterium atoms was studied for a HD–D_2–He sample, while the tunnelling reaction (4) was occurring. The time dependence of these ratios for H and D

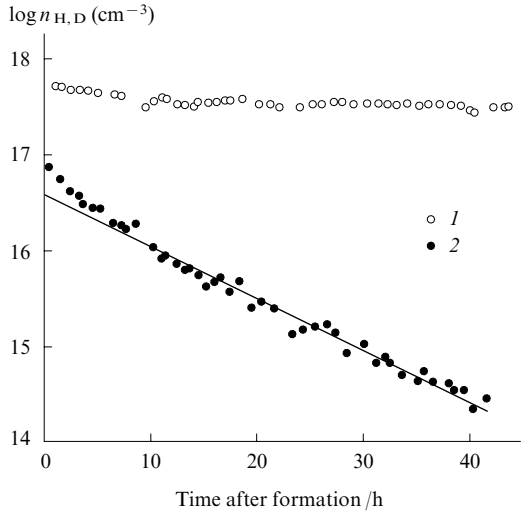


Figure 9. Time dependence of the logarithms of the average concentration of H atoms (*1*) and D atoms (*2*) in HD–D_2–He solids immersed in superfluid helium at $T = 1.35$ K.[51]
Sample was prepared from $H_2 : D_2$: He = 1 : 4 : 100 gas mixture.

atoms is shown in Fig. 10. It was found that for H atoms, the ratio is equal to 0.11 and this value remains essentially constant during the course of the reaction. Thus, by Eqn (9), the average number of HD molecules surrounding H atoms in the sample does not change during the experiment. Due to the tunnelling reaction (5), a hydrogen atom might migrate to the next site in the solid matrix and possibly meet another hydrogen atom, which could lead to recombination and decay of the hydrogen atom concentration. However, this process is predicted to be $\sim$ 200 times slower than the diffusion of H through H_2 by tunnelling.[12] The observed stability of hydrogen atoms in the sample being discussed is not yet completely understood. Additional studies of the immediate environment of the stabilised atoms are needed for further elucidation of the nature of the tunnelling reactions.

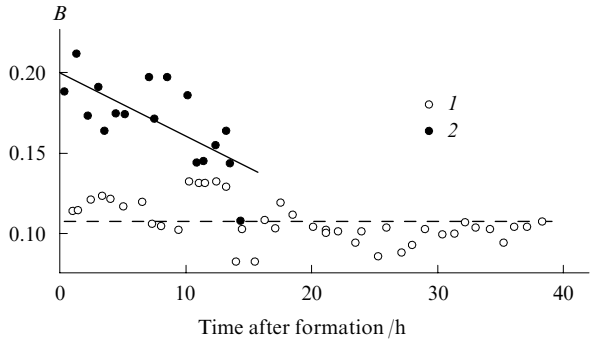


Figure 10. Time dependence of the ratio of the intensities of the satellite and the main lines (*B*) for hydrogen atoms (*1*) and deuterium atoms (*2*) in HD–D_2–He solids stored at $T = 1.35$ K.[51]

In contrast, for D atoms the ratio was reduced from 0.2 to 0.14 in 14 h, showing that the number of HD molecules surrounding D atoms is decreased by 30%. The D atoms consume HD and release H atoms. The rate process is complicated by the fact that the D atoms exist in a variety of sites having between zero and twelve neighbouring HD molecules. The population of these sites initially follows a binomial distribution, with 40% of the neighbours of the D atoms being

HD and the remainder being D_2. The lifetime of a D atom in a given site is inversely proportional to the number of HD neighbours, so that over time the distribution of sites becomes skewed toward D atoms occupying sites with fewer HD nearest neighbours that show smaller satellite line ratios.

3. Pulsed ESR studies of H and D atoms in clusters forming Im–He solids

The CW method suffers from a high degree of inhomogeneous line broadening due to the neighbouring nuclei and atomic radicals. As we mentioned earlier, this broadening obscures the observation of satellite lines associated with transitions involving the spin flip of an electron and a simultaneous spin flip of a deuteron on a neighbouring HD or D_2 molecule. The standard pulsed ESR method of echo refocusing provides a means to study these weak couplings within inhomogeneously broadened systems. As discussed earlier, a homemade pulsed homodyne X-band spectrometer, designed for the study of atoms in Im–He solids, was used in the experiments at Cornell.[45] A primary echo sequence of $90^\circ-\tau-180^\circ-\tau-$echo with a 90° pulse length of 40 ns was used. To obtain the dependence of the amplitude of spin echo signals on the time between subsequent pulse pairs, τ was varied from 460 ns to 12 μs, while the recovery time t between successive pulse sequences was held constant at 400 ms. The method of ESEEM proved to be a powerful technique for observing spin flips on neighbouring deuterons. The first experiments were performed on $D-D_2-He$ samples prepared from a gas mixture with a ratio $D_2:He = 1:20$. Figure 11 displays the experimental electron spin echo amplitude *vs.* τ, giving the ESEEM trace along with the simulated one for the low field hyperfine line of the D atom. The echo signal intensity decreased monotonically and was strongly modulated by the first and second harmonics of the Larmor frequency of deuterons in the molecules near the D atoms. The applied magnetic field couples to the deuterons much more strongly than the field due to the electron spins, so the applied magnetic field determines the ~ 2 MHz Larmor frequency of the deuterons. The amplitude of the modulation depends on the number of deuterons surrounding the D atoms and their proximity to those atoms. The amplitude of modulation is also proportional to $I(I+1)$, where I is the nuclear spin quantum number of the molecule interacting with the D atom. Therefore the amplitude of modulation of ESEEM signals for atoms surrounded by D_2 molecules with $I = 2$ and $I = 1$ should be much larger than for the case of atoms surrounded by protons (as a constituent of HD) with $I = 1/2$. This difference is especially pronounced at low temperatures because the ground state of D_2 is predominantly of the $I = 2$ form and conversion to the ground state occurs rapidly in the vicinity of the unpaired electron spins of the hydrogen and deuterium atoms. The ESEEM signal associated with the proton moment has not been observed in our experiments.

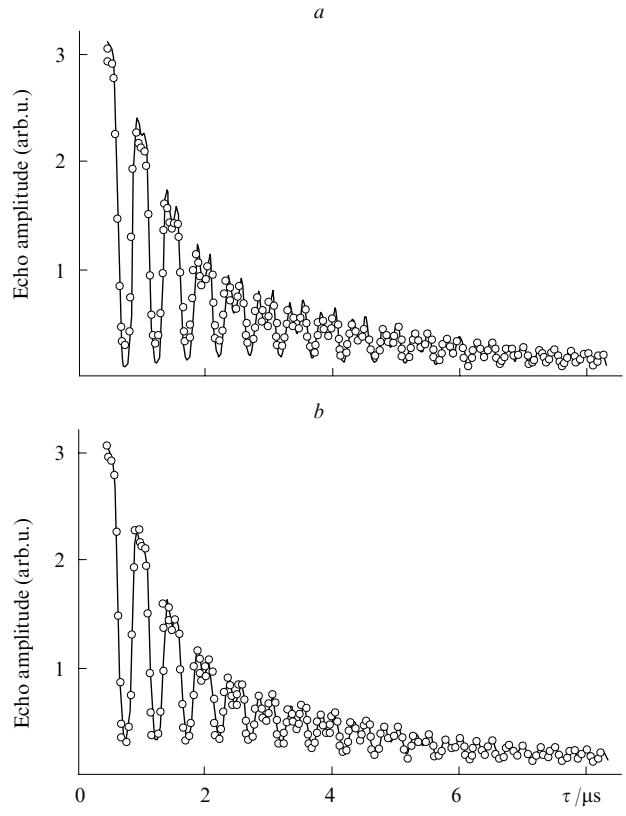


Figure 11. Two-pulse ESEEM trace of the low field hyperfine line of D in D_2–He sample.[54] (*a*) The circles show every fourth data point. The line shows the best fit of the bulk population model. (*b*) The circles show every fourth data point. The line shows the best fit of the two population (bulk and surface) model $E(\tau)$.

For analysis of the experimental ESEEM data the model used initially was that developed by Kumada *et al.*[31] to study D atoms in bulk D_2. They simulated their ESEEM signals with the standard theoretical results for orientationally disordered crystalline systems.[55] This model assumes that all possible orientations of the face centred cubic (fcc) deuterium crystal axis with respect to the applied magnetic field are equally represented within the sample. The Hamiltonian includes terms representing electron–nuclear interactions through dipolar magnetic coupling and an isotropic superhyperfine coupling due to the contact interaction of the electronic wave function with the nuclear wave function of the nearest neighbouring molecules. No internuclear couplings are included; as a result, the echo modulation due to the presence of several nuclei surrounding the electron spin is simply the product of the modulation due to each individual nucleus.

The echo signal as a function of the interpulse time τ was modeled as:

$$E(\tau) = E_{\mathrm{dec}}(\tau)E_{\mathrm{b}}(\tau),$$

$$E_{\mathrm{b}}(\tau) = \prod_{i=1}^{5}\langle E_i(\tau)\rangle_\theta^{N_i},$$

$$E_{\mathrm{dec}}(\tau) = A\mathrm{e}^{-\tau/T_2},$$

where $E_{\mathrm{dec}}(\tau)$ contains the characteristic exponential decay time T_2 of the electron spin echo and $E_{\mathrm{b}}(\tau)$ represents the modulation of the echo due to the N_i molecules populating the closest five coordination shells $i = 1-5$ around the electron spin. The modulation functions $E_i(\tau)$ due to each individual molecule are averaged over all orientations before they are multiplied. This unphysical feature of the model is computationally expedient and causes only slight changes in the predicted echo signals for systems with weak electron–nuclear couplings such as hydrogen or deuterium atoms substitutionally positioned within a deuterium matrix.[56]

At liquid helium temperatures D_2 can exist in ortho- and para-states corresponding respectively to the $J = 0$ and $J = 1$ rotational states of the molecule. The para state is 85 K more energetic than the ortho-state but its conversion to the ortho-state is highly forbidden. Deuterons are bosons, so the product of the spatial and spin wave functions of the deuterons must be symmetric under particle exchange. The allowed molecular spin states are then $I = 0$ and $I = 2$ for ortho-deuterium and $I = 1$ for para-deuterium. The energy difference between the $I = 0$ and $I = 2$ states is extremely small compared to the

thermal energy, so the populations of the states are determined by their degeneracy. As there are five orientations of the $I = 2$ state and one orientation of the $I = 0$ state, 5/6 of the ortho-deuterium molecules are in the $I = 2$ spin state, while 1/6 of the ortho-deuterium molecules are in $I = 0$ spin state. The para-to-ortho relaxation of deuterium is catalysed by the magnetic field gradients produced by paramagnetic species, so that all of the deuterium molecules in the nearby coordination shells around a D atom can be assumed to be of the ortho-form. As the $I = 0$ molecules are not magnetically active, the number of molecules in each coordination shell must be adjusted accordingly. For example, for an atom substitutionally positioned in D_2 fcc, the first shell of twelve nearest neighbours is modelled with ten spin-2 particles, each possessing the Larmor frequency of the deuteron.

Ponti[57] has shown that Chebyshev polynomials of the second kind relate the ESEEM modulation function due to a particle of any spin to the modulation function that would result if that particle were spin 1/2. Specifically,

$$E_i(\tau) = \frac{1}{2I+1} U_{2I}[V_i(\tau)],$$

where U_n is the nth Chebyshev polynomial of the second kind and $V_i(\tau)$ is the spin 1/2 modulation function. Finally, the explicit form of $V_i(\tau)$ is

$$V_i(\tau) = \frac{K}{2}\Big[1 - \cos(\omega_\alpha \tau)\Big]\Big[1 - \cos(\omega_\beta \tau)\Big],$$

$$K = \left(\frac{B\omega_{\mathrm{L}}}{\omega_\alpha \omega_\beta}\right)^2,$$

$$B = 3g_{\mathrm{n}}\beta_{\mathrm{n}}g_{\mathrm{e}}\beta_{\mathrm{e}}\frac{\cos\theta\sin\theta}{\hbar(r_i)^3},$$

$$\omega_{\mathrm{L}} = g_{\mathrm{n}}\beta_{\mathrm{n}}H_0,$$

$$\omega_\alpha = \left[\left(\frac{A}{2} + \omega_L\right)^2 + \left(\frac{B}{2}\right)^2\right]^{1/2},$$

$$\omega_\beta = \left[\left(\frac{A}{2} - \omega_L\right)^2 + \left(\frac{B}{2}\right)^2\right]^{1/2},$$

$$A = g_{\mathrm{n}}\beta_{\mathrm{n}}g_{\mathrm{e}}\beta_{\mathrm{e}}\frac{3\cos^2\theta - 1}{\hbar(r_i)^3} + 2\pi a_{\mathrm{sup}},$$

where r_i is the distance from the electron to coordination shell i, θ is the angle between the applied field H_0 and the vector pointing from the radical to the molecule, g_e and g_n are the g-factors of the electron and nuclear spins, β_e and β_n are the Bohr and nuclear magnetons, and a_{sup} is the isotropic super-hyperfine coupling.

Kumada *et al.*[31] fitted a_{sup} and r_I to their data obtained from pure irradiated solid deuterium for two sets of N_i and r_i. One set corresponded to the environment around substitutional sites in the D_2 fcc lattice and the other set corresponded to the environment around interstitial sites. The predicted modulation functions were radically different (the interstitial sites have much deeper modulation due to the smaller nearest neighbour distances) and it was immediately clear that the D atoms reside in the substitutional sites. Numerical fitting gave $r_i = 3.6$ Å, corresponding to the nearest neighbour spacing of the unstrained molecular lattice, and $a_{\mathrm{sup}} = 70$ kHz.

Applying the above model to our Im – He solid gave poor agreement with the data obtained for the D – D_2 – He sample as presented in Fig. 11 *a*. For Im – He solids it is reasonable to suggest that atoms are stabilised not only inside molecular clusters, but also on the surfaces of these clusters. Following this suggestion, the experimental ESEEM data were fitted with two decaying exponentials multiplied with two oscillatory modulation terms:

$$E(\tau) = A\Big[Qe^{-\tau/T_{2\mathrm{Q}}} + (1-Q)\mathrm{e}^{-\tau/T_{2\mathrm{L}}}\Big]\Big[bE_{\mathrm{b}}(\tau) + (1-b)E_{\mathrm{s}}(\tau)\Big],$$

where A, Q, $T_{2\mathrm{Q}}$ and $T_{2\mathrm{L}}$ parameterise the echo decay and b weights the modulation functions E_{b} and E_{s}.[54] The function E_b simulates the ESEEM signal of D atoms within the solid clusters by assuming they are substituted into an fcc lattice composed of D_2 molecules. The modulation signal E_{b} produced by atoms positioned within deuterium nanoclusters was identical to that described above for atoms substituted in bulk deuterium. The function E_{s} is produced by the same model, but with the population of each coordination shell around the atom reduced by one-half. This simulates D atoms at the surfaces of the clusters in contact with the helium. We fixed r_i and a_{sup} to the values found to describe bulk deuterium so that our modulation function contained only one free parameter, the ratio of atoms within the deuterium nanoclusters to atoms at the cluster – helium interface. The functional form of the echo decay was found empirically to fit the data well with a small number of parameters. Notably, modelling the data with separate decay functions for the bulk and surface terms results does not improve the fits.

As a result of applying the modified model, the two-pulse ESEEM measurements presented in Fig. 11 *b* were well described by fits that placed 50% – 60% of the deuterium atoms at the interface between the molecular deuterium nanoclusters and the superfluid liquid helium.[54] The rest of the atoms occupy substitutional sites within the nanoclusters. These pulsed ESR measurements provide the first direct indication that a large fraction of the atomic radicals within impurity – helium solids reside on the cluster – helium interfaces, as first suggested by Gordon.[58] This result implies that some mechanism causes the deuterium atoms to preferentially occupy the nanocluster surfaces, whereas a random substitution of the deuterium molecules of the clusters would only place 10% – 20% of the atoms at the cluster – helium interface, depending on the cluster size.

The measurements of ESEEM signals by pulsed ESR provide complementary information about deuterons surrounding H and D atoms in solid mixtures of hydrogen isotopes that cannot be provided by CW ESR due to the small deuteron magnetic moment. The ESEEM signal associated with ESR studies of H atoms in a HD – D_2 – He solid produced from an initial gaseous mixture $H_2 : D_2 : He = 1 : 4 : 100$ is shown in Fig. 12 *a*. For the analysis of the ESEEM data, the model applied for D – D_2 – He solid was modified to account for the presence of D_2 and HD molecules surrounding the atoms, with the ratio of HD and D_2 molecules allowed to vary as a fitting parameter. The fraction of atoms at the surface was assumed to be 55%, the same as was found in the D_2 – He solid.[54] The best fit in a model calculation of the ESEEM signal of the H atoms, which is represented as a solid line in Fig. 12 *a*, was obtained for a configuration in which ten deuterium and two HD molecules surrounded the H atoms.[59] The ESEEM signals for H atoms recorded at the beginning of the experiment and 6 hours later were identical, showing that the number of D_2 and HD molecules surrounding the H atoms did not change as the reaction proceeded. This result was in agreement with previously described CW experiments in which the satellite amplitudes remained unchanged throughout the experiment.[51]

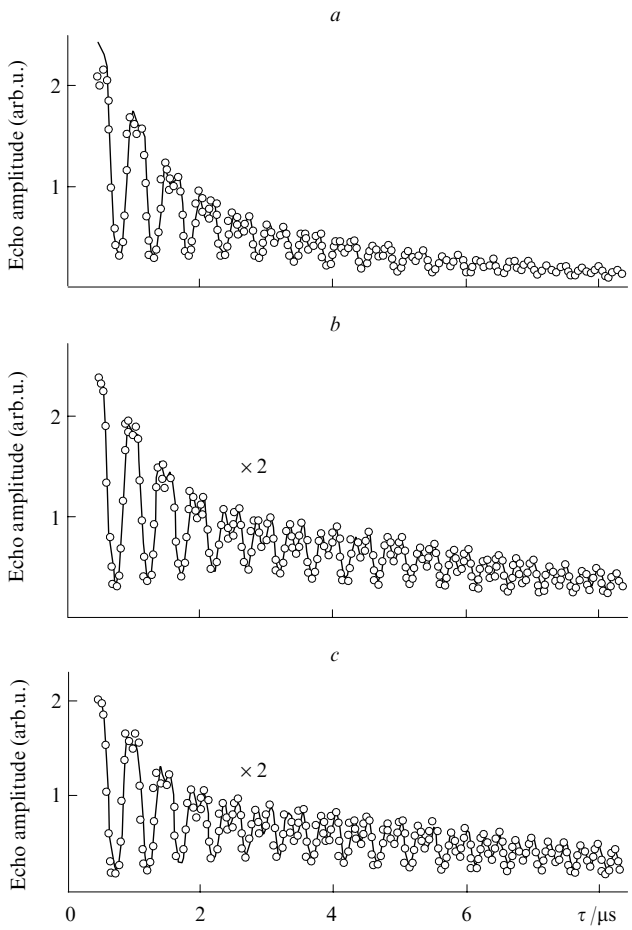


Figure 12. Two pulse ESEEM signals (circles) for the H and D atoms in $HD-D_2-He$ solid at 1.35 K taken at 8.93 GHz: (*a*) low field hyperfine component of H atoms at 2910.1 G; (*b*, *c*) low field hyperfine components for D atoms at 3105.5 G at the beginning of the experiment and six hours later, respectively.
Solid lines are the best fits of model calculations to the experimental data (see text).[59]

The ESEEM data for D atoms show that their number decreases over the course of the tunnelling reaction (see Figs 12*b* and 12*c*). Modelling of the ESEEM signals for D atoms in the $HD-D_2-He$ solid obtained at the beginning of the experiment (solid line in Fig. 12*b*) shows that nine D_2 and three HD molecules surrounded a typical D atom within the bulk of the cluster. The same model shows that six hours later (see Fig. 12*c*) ten D_2 and two HD molecules surrounded a typical D atom. This result is also in good agreement with the results obtained from CW ESR measurements discussed earlier, which suggested that the number of protons (and thus the number of HD molecules) surrounding the D atoms decreases by about 30% in the first six hours following the formation of the sample obtained from the $H_2:D_2:He = 1:4:100$ gas mixture.

In conclusion, the CW and pulsed ESR methods provide complementary information about the trapping sites and the changing environment of atoms participating in low temperature tunnelling reactions. This information is particularly important for elucidation of the mechanisms of tunnelling reactions of hydrogen atoms.

IV. Studies of H atoms in solid H_2 films at ultralow temperatures

The methods for creating systems of matrix isolated hydrogen atoms mentioned above led to the formation of highly inhomogeneous solids with many defects. In all of these methods one gets quite irregular solids, where the diffusion of the atoms is mediated by inhomogeneities of the crystalline field.

A novel method of ultra-slow deposition of films of solid H_2 with embedded hydrogen atoms has been recently discovered in experiments with spin polarised atomic hydrogen gas.[42] It is well known that spin-polarised atomic hydrogen gas can be stabilised at temperatures approaching absolute zero (see Ref. 60 and references therein). Atoms are stabilised by applying a strong magnetic field and lining the walls of the experimental cell with a superfluid helium film, thus preventing adsorption of the atoms. The schematic of a typical experimental setup for studies of spin-polarised H gas (H↓) is presented in Fig. 13. Atomic hydrogen gas is produced in a cryogenic radiofrequency dissociator, and the high field-seeking fraction (H↓) is pulled into the sample cell located in a 4.6 T magnetic field. The typical flux of atoms entering the sample chamber (SC) (see also Fig. 14*a*) is $\sim 2\times 10^{13}$ s^{-1}. With the continuously operating dissociator, bulk gas densities up to 2×10^{15} cm^{-3} can be accumulated in the SC at a temperature of $\sim$ 350 mK. H↓ atoms of both lowest hyperfine states *a* and *b* (Fig. 14*b*) are accumulated in equal amounts. The H↓ samples were not perfectly stable against recombination of the atoms into H_2 even in very strong (> 10 T) magnetic fields due to the unavoidable three-body recombination channel. The molecules resulting from recombination stick to the walls of the experimental chamber and slowly form a layer of solid H_2. This layer in the experiments with H↓ helps to reduce the decay rate of the sample due to one-body nuclear relaxation. A typical rate for solid H_2 film growth is very slow, 0.5–1 molecular layer per hour, which is mainly limited by the efficiency of the radiofrequency dissociator.

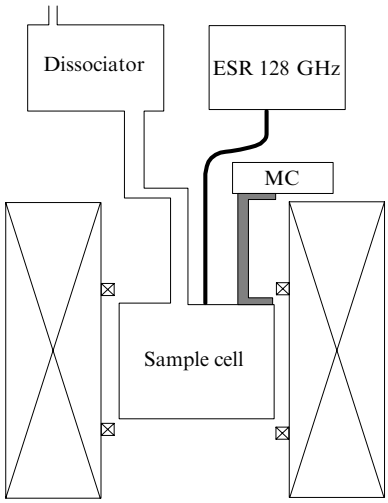


Figure 13. Block diagram of the setup for investigations of H atoms in solid H_2 at ultralow temperatures.
The label MC denotes the mixing chamber of the $^3He-^4He$ dilution refrigerator.

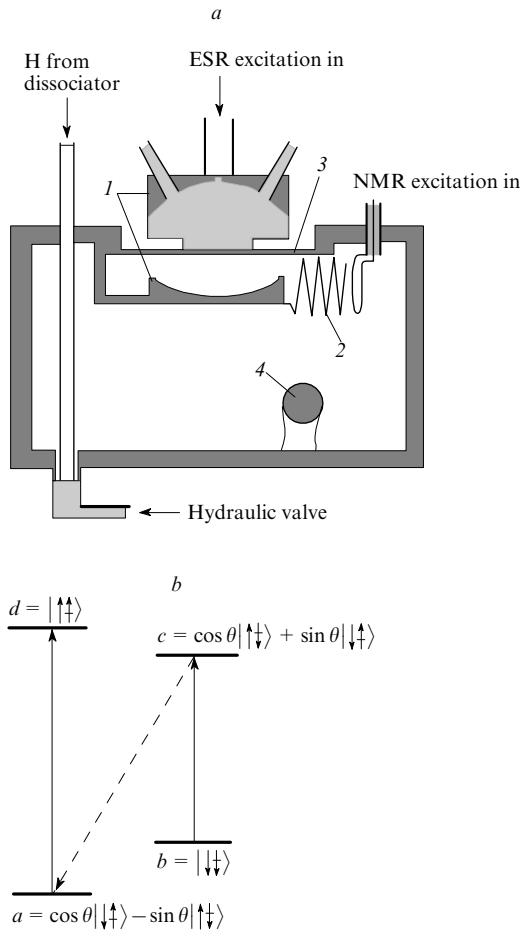


Figure 14. Schematic drawing of the sample cell (*a*); hyperfine level diagram for hydrogen atom in a strong magnetic field (*b*).[42]
(*a*) Fabry–Perot ESR resonator (*1*), helical NMR resonator (*2*), Mylar foil (*3*), quartz microbalance crystal (*4*). (*b*) Arrows denote electron and nuclear spin projections. The values of the angles θ are determined from the equation $\tan 2\theta = a/[h(\gamma_e + \gamma_p)H]$, where a is the hyperfine constant, H is the magnetic field and γ_e, γ_p are the electron and proton gyromagnetic ratios, respectively.

It has been found that H atoms are captured inside the solid H_2 films covering the SC walls.[42] The mechanism of this process is not known. One of the possibilities is that the molecules appear in the gas phase in one of the highest ro-vibrational states [61] and may transfer their energy to the atoms in binary collisions. The energy acquired by the atom in such an event can exceed the potential barrier for the atoms to penetrate into the helium film ($\sim$40 K), and therefore the atom can punch through the film and stick to the solid H_2. It has been verified that the atoms do not appear in the sample cell as a result of diffusion from the dissociator along the solid H_2 film covering the surface of the fill line. Closing the hydraulic valve at the cell bottom stopped the growth of the atomic ESR signal. Although very slow, this method of deposition of films of H_2 with embedded H atoms has a number of advantages in comparison with the traditional methods of creating such systems employed earlier. The system is absolutely free of any possible impurities, since no other gas, except H$\downarrow$ can exist at temperatures below 1 K. Although some small admixtures ($< 10^{-4}$) of spin-polarised deuterium can be generated in the dissociator, they cannot reach the sample cell passing through the 0.5 m long filling line, since the recombination rates for D are $> 10^3$ times larger than for H. Another advantage of this method is that the deposition rate and average energy flux into the system is so slow that one may expect to obtain solid crystals with the least amount of internal crystalline defects, thus making this system very close to ideal for studies of quantum diffusion and tunnelling chemical reactions.

Due to the strong magnetic fields needed for the stabilisation of H$\downarrow$, high frequency (128 GHz) ESR and 910 MHz NMR and ENDOR methods were used to characterise the samples. The H_2 films containing H atoms were situated on the surface of the Mylar foil and on the lower spherical mirror (see Fig. 14*a*), both located at antinodes of the Fabry–Perot resonator (FPR) operating in the TEM_{005} mode (see Refs 43 and 60 for more details of the experimental setup).

The ESR spectrum of H atoms in solid H_2 in the applied magnetic field of 4.6 T basically consists of two lines separated by 507 G due to the hyperfine interaction. In Fig. 15 (upper trace) the ESR spectra of the lower field line of H atoms in solid H_2 are presented together with the corresponding line originating from the atoms of the gas phase above the film obtained at $T \sim 350$ mK. Special shim coils were used to minimise the magnetic field inhomogeneity, or *vice versa*, to increase the gradient and resolve the absorption lines originating from the atoms located on the Mylar foil and the lower mirror. Integrals of these lines were equal to each other, which indicates a homogeneous film coating over the sample cell walls. Having the possibility to resolve the lines from the free atoms in the gas phase and the matrix isolated ones, one can obtain useful information about the influence of the crystal environment on the *g*-factor and the hyperfine constants. The ESR lines of H atoms in solid H_2 were found to be shifted by $\sim$0.28 G towards the centre of the spectrum compared with those of free atoms (see Fig. 15) with the magnitude of the shift being the same for both ESR lines. Therefore, the atoms in the solid have the same value of the *g*-factor and a somewhat reduced hyperfine interaction.

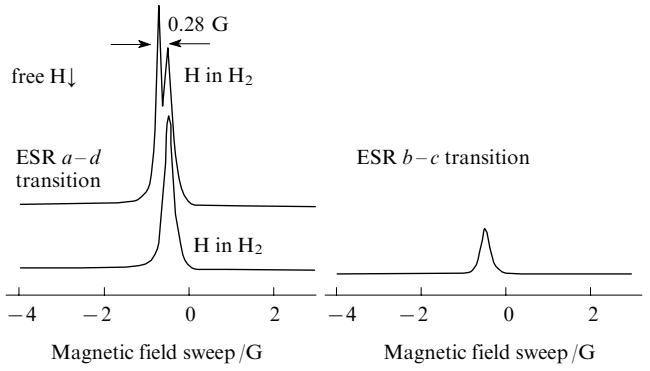


Figure 15. ESR spectra of the H$\downarrow$ gas and of H atoms in the solid H_2 matrix observed in the measurements: upper left trace is small H$\downarrow$ density $\sim 2 \times 10^{13}$ cm^{-3} (left peak) together with the H in solid H_2 line (right peak); bottom traces are H in solid H_2 spectrum.[42]
Note that the $a-d$ transition signal is larger than the $b-c$ transition signal.

To manipulate the populations of the states *a* and *b*, nuclear spin transitions were induced by applying resonant excitation to the helical 910 MHz resonator (HR) located on the side of the FPR (see Fig. 14*a*). Due to the small number of atoms in the sample and the poor sensitivity of NMR, it is not possible to detect the NMR absorption directly. However, one can detect it through the change of the ESR signal associated with the change of the populations of hyperfine states. For observation of such double resonance spectra, the allowed

electron $b-c$ transition was saturated with high excitation power while the ESR sweep was stopped in the middle of the H in H_2 line. Then a radiofrequency signal was applied to the helical NMR resonator (HR) with its frequency swept through the position of the nuclear $a-b$ transition (near 909 MHz). The power absorbed by the ESR is increased once the nuclear resonance condition is reached, since the atoms are transferred from the a to the b state (Fig. 16). The position of the ENDOR line relative to that of the free atoms gives the value of the hyperfine constant change $-1320(10)$ kHz. This reduction of the hyperfine constant with respect to the free atoms implies that the atoms are situated in substitutional sites. In this case the effects of van-der-Waals attraction to the neighbouring molecules dominate over the Pauli repulsion.[62] A similar conclusion has been made in the ENDOR studies of Nagoya group[30] for the H in H_2 samples obtained by a different method. A remarkable feature of the ENDOR spectra observed in the films of H in H_2 created by the slow deposition method[42] is the unusually small width of the NMR transition (~ 15 kHz). This provides good evidence of the high quality of the H_2 crystals obtained by this method.

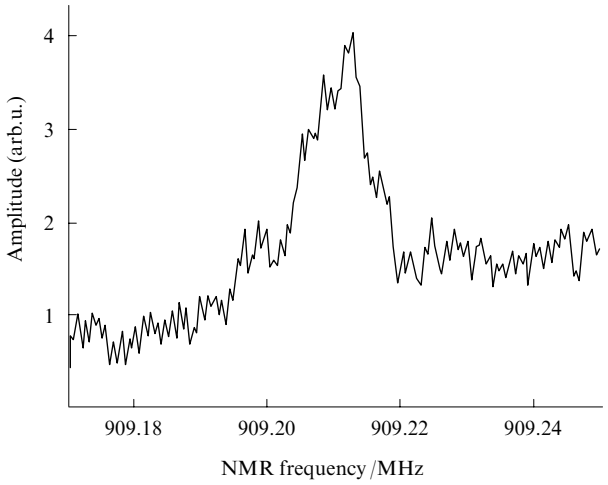


Figure 16. ENDOR spectrum of hydrogen atoms in solid H_2.[42]

Another interesting feature found in the experiments with the H in H_2 films[42] was the very high stability of the atoms to recombination (Fig. 17) at temperatures below 150 mK. For this temperature range no decay of H atoms was detected over a period of at least two weeks. A slow decrease of H atom concentration has been observed at 300 mK and 480 mK. Figure 18 shows the values of the recombination rate constants obtained in these experiments compared with the previous higher temperature results and with the theoretical predictions. It has been found that for temperatures below 0.9 K the recombination rate constants, $k_H(300\ \text{mK}) = 1.5\times10^{-25}\,\text{cm}^{-3}\,\text{s}^{-1}$ and $k_H(480\ \text{mK}) = 3\times10^{-25}\,\text{cm}^{-3}\,\text{s}^{-1}$ are much smaller than predicted theoretically[7,63] and found in previous experiments[8] at $1.35 < T < 4.2$ K. However, at the highest temperatures (900 mK) used in the studies of the H in H_2 films[42] the rate constant increased substantially and came into close agreement with extrapolation of the previous results. The vanishingly small recombination at the lowest temperatures makes it promising to achieve extremely low temperatures for this metastable system in future experiments, since recombination heating would not be a factor.

Populations of the lower hyperfine states can be manipulated by saturation of the ESR or NMR transitions. Saturating the $b-c$ transition leads to the pumping of the atoms from the state b to a (*via* the Overhauser effect) through the relaxation of

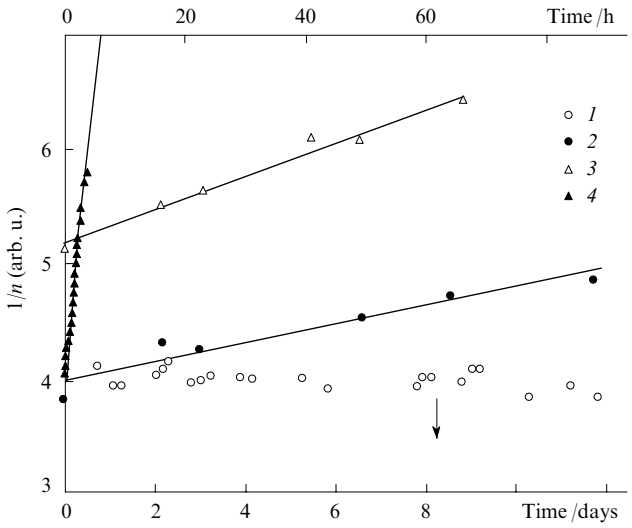


Figure 17. Decay of H in H_2 sample at different temperatures.[42] T/mK: (*1*) 150 (lower time scale), (*2*) 300, (*3*)480, (*4*) 900 (all upper time scale).

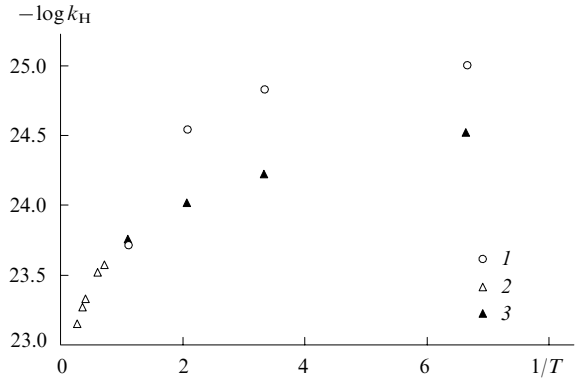


Figure 18. Temperature dependence of logarithm of rate constant for recombination of H atoms in solid H_2: our experimental results at $T < 1$ K (*1*), experimental results[8] for the temperature range $1.3 < T < 4.2$ K (*2*) and theoretical prediction for $T < 1$ K (*3*).[7]

the partially forbidden $a-c$ transition. The relaxation time of the $a-c$ transition of H atoms inside H_2 films is about 3 s. Using the Overhauser effect, one can transfer the entire population to the a state within several seconds. Then the a and b populations can again be equalised by applying resonance power to the $a-b$ transition. Recovery of the population ratio n_a/n_b or the polarisation

$$p = \frac{n_a - n_b}{n_a + n_b}$$

to the equilibrium value is controlled by the nuclear relaxation process which turns out to be very slow, $t_{b-a} \sim 60-80$ h at 150 mK (Fig. 19). A most intriguing observation in the experiment of Ref. 42 was the non-Boltzmann population of the hyperfine states b and a in the steady state. The populations ratio is typically characterised by the value of nuclear polarisation. The value of $p(t\to\infty) = 0.5(1)$ observed at $T = 150$ mK was much larger than $p \approx 0.14$ dictated by the Boltzmann statistics with $n_a/n_b = \exp(E_{a-b}/T)$, with $E_{a-b} \approx 43$ mK being the energy difference between the a and b states. The

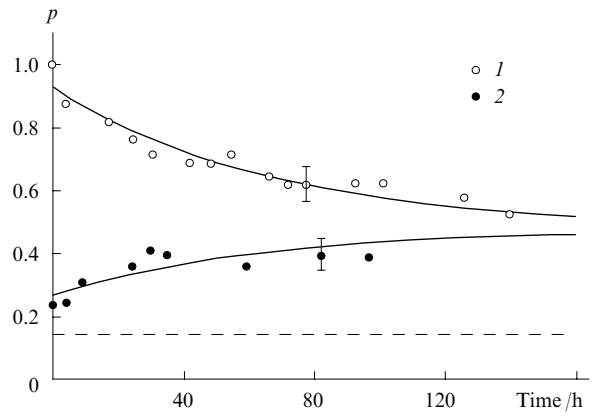


Figure 19. Evolution of the nuclear polarisation $p = (n_a - n_b)/(n_a + n_b)$ at $T = 150$ mK after saturation of the $b-c$ transition (*1*) and after partial saturation of the $a-b$ transition (*2*). The horizontal dashed line marks the nuclear polarisation corresponding to a thermal (Boltzmann) ratio $n_a/n_b = \exp(E_{a-b}/T)$ with $T = 150$ mK.[42]

non-equilibrium population ratio observed in these experiments can be explained by the possible formation of a Bose–Einstein condensate (BEC) in the ensemble of atoms. This cannot occur if the atoms are evenly distributed over the crystal because the average density is not high enough to reach quantum degeneracy. If however, there are regions in the crystal with much higher local concentrations, the condensation may happen there and the system should then consist of two kinds of atoms, those in the high concentration regions and those in the rest of the crystal.

A powerful concentrating mechanism such as the phase separation seen in solid ^{3}He–^{4}He mixtures [64, 65] and potentially in ortho-para solid H_2 mixtures [66, 67] is required to reach a concentration of $\sim 5 \times 10^{20}$ cm^{-3}, which corresponds to a BEC onset temperature of 0.2 K for H atoms with effective mass 3.5 m_H as calculated from the experimental n_a/n_b population ratio. Diffusion of the H atoms *via* exchange tunnelling can be considered as a motion of 'quasivacancies', leading to a broad energy band and low effective mass.[68] One might imagine that the H atom rich phase exists in small bubbles or layers surrounded by the H atom starved phase.

V. Conclusions and future work

Impurity–helium solids are highly porous gel-like nanomaterials consisting of interconnecting clusters of impurities with a characteristic size 5–9 nm and an average density over the entire sample volume as low as 10^{20} atoms (molecules) cm^{-3}. In fact, Im–He solids are a collection of nanoclusters. One cubic centimeter of a typical Im–He sample contains a large number ($\sim 10^{16}$) of clusters, each consisting of $\sim 10^4$ molecules and 10–100 or more stabilised atoms. Therefore, it is possible to study simultaneously a large collection of nanoreactors, in which low temperature chemical reactions can be investigated.

The kinetics of exchange tunnelling reactions of hydrogen isotopes were studied in nanoclusters immersed in superfluid helium at $T = 1.35$ K. The rate constants for different reactions have been determined and the changes of the environments of hydrogen and deuterium atoms in the course of these reactions have been studied. The rate constants for reactions (2) and (4) in nanoclusters were found to be similar to those obtained in bulk solids. In contrast, the rate constant for the reaction (1) in nanoclusters is an order of magnitude higher as compared to that obtained in bulk solid hydrogen. Possibly the recombination of H atoms occurs primarily on the surfaces of the nanoclusters. The analysis of the pulsed ESR data shows that 50%–60% of all stabilised atoms reside on the surfaces of the nanoclusters.

Reactions between hydrogen atom isotopes might be studied at even lower temperatures. This would shed more light on the details of tunnelling processes in chemical reactions occurring in the solid phase. The study of Im–He solids at ultralow (10–20 mK) temperatures should be pursued. Obviously, such a program will encounter major technological challenges to adapt methods of preparation of Im–He solids with high concentrations of stabilised atoms to the restrictions existing in a dilution refrigerator cryostat. Nevertheless, such investigations could show great promise. Cooling down the H–H_2–He samples with high concentrations of stabilised H atoms to the temperature region of 10–20 mK could lead to the observation of Bose–Einstein condensation of H atoms.

Another approach to studies of the kinetics of recombination of H atoms in H_2 solids at ultralow temperatures was demonstrated. The technique usually used for studies of spin-polarised hydrogen gas also provided the opportunity to prepare and investigate H atoms in thin molecular films of solid H_2 . For the first time, the recombination rates of H atoms in solid H_2 were studied in the temperature range 0.15–0.9 K. It was found that recombination rate constants are significantly smaller at these temperatures than was predicted theoretically. Moreover, at $T = 0.15$ K, H atoms were very stable during two weeks of observations. At this temperature the population of the lowest hyperfine state of atomic hydrogen was found to be much larger that that expected from the Boltzmann distribution. A possible explanation for this observation is achievement of the Bose–Einstein condensation of H atoms in solid H_2. This might be possible if regions of high local concentration of H atoms can be created in solid H_2. Additional studies of the temperature dependence of the populations of the lowest energy levels of H atoms are necessary to confirm whether BEC is actually occurring in this system. Alternative explanations should also be explored in future experiments and theoretical work.

We would like to thank the National Science Foundation (Grant No. DMR-0504683), NASA (Grant No. NAG3-2871) and CRDF (Grant No. RUP1-2841-CG-06) for support prior to and during the preparation of this review. We also are grateful to the Academy of Finland (Grant No. 206109) and the Wihuri Foundation for supporting the research program at Turku University. One of us (D M Lee) would like to thank the Aspen Center for physics, which provided a forum for interesting discussions. The authors take this opportunity to express their gratitude to R Boltnev, S Kiselev, P Borbat, J Freed, E Müller, V Kiryukhin, J Jarvinen, J Ahokas and E Vehmanen for stimulating and useful discussions.

References

1. C K Jen, S N Foner, E L Cochran, V A Bowers *Phys. Rev.* **104** 846 (1956)
2. C K Jen, S N Foner, E L Cochran, V A Bowers *Phys. Rev.* **112** 1169 (1958)
3. L A Wall, D W Brown, R E Florin *J. Phys. Chem.* **63** 1762 (1959)
4. L H Piette, R C Rempel, H E Weaver, J M Flournoy *J. Chem. Phys.* **30** 1623 (1959)
5. A M Bass, H P Broida *Formation and Trapping of Free Radicals* (New York, London: Academic Press, 1960)
6. A F Andreev, I M Lifshits *Zh. Eksp. Teor. Fiz.* **29** 1107 (1969) [a]
7. Yu Kagan, L A Maksimov, N V Prokofev *Pisma Zh. Eksp. Teor. Fiz.* **36** 204 (1982) [b]
8. A V Ivliev, A Ya Katunin, I I Lukashevich, V V Sklyarevskii, V V Suraev, V V Filippov, N I Filippov, V A Shevtsov *Pisma Zh. Eksp. Teor. Fiz.* **36** 391 (1982) [b]

9. H Tsuruta, T Miyazaki, K Fueki, N Azuma *J. Phys. Chem.* **87** 5422 (1983)
10. E B Gordon, A A Pelmenev, O F Pugachev, V V Khmelenko *Pisma Zh. Eksp. Teor. Fiz.* **37** 282 (1983) [b]
11. R N Porter, M Karplus *J. Chem. Phys.* **40** 1105 (1964)
12. T Takayanagi, K Nakamura, S Sato *J. Chem. Phys.* **90** 1641 (1989)
13. T Kumada *Phys. Rev. B* **68** 052301 (2003)
14. M Sharnoff, R V Pound *Phys. Rev.* **132** 1003 (1963)
15. A S Iskovskikh, A Ya Katunin, I I Lukashevich, V V Sklyarevskii, V V Suraev, V V Filippov, N I Filippov, V A Shvetsov *Zh. Eksp. Teor. Fiz.* **64** 1085 (1986) [a]
16. T Miyazaki, K-P Lee, K Fueki, A Takeuchi *J. Phys. Chem.* **88** 4959 (1984)
17. K-P Lee, T Miyazaki, K Fueki, K Gotoh *J. Phys. Chem.* **91** 180 (1987)
18. T Miyazaki, N Iwata, K-P Lee, K Fueki *J. Phys. Chem.* **93** 3352 (1989)
19. E B Gordon, A A Pel'menev, O F Pugachev, V V Khmelenko *Fiz. Nizk.Temp.* **11** 307 (1985) [c]
20. E P Bernard, R E Boltnev, V V Khmelenko, V Kiryukhin, S I Kiselev, D M Lee *J. Low Temp. Phys.* **134** 169 (2004)
21. E P Bernard, R E Boltnev, V V Khmelenko, V Kiryukhin, S I Kiselev, D M Lee *Phys. Rev. B* **69** 104201 (2004)
22. A V Ivliev, A S Iskovskikh, A Ya Katunin, I I Lukashevich, V V Sklyarevskii, V V Suraev, V V Filippov, N I Filippov, V A Shevtsov *Pisma Zh. Eksp. Teor. Fiz.* **38** 317 (1983) [b]
23. T Miyazaki, K-P Lee *J. Phys. Chem.* **90** 400 (1986)
24. T Miyazaki, S Mori, T Nagasaka, J Kumagai, Y Aratono, T Kumada *J. Phys. Chem. A* **104** 9403 (2000)
25. T Kumada, S Mori, T Nagasaka, J Kumagai, T Miyazaki *J. Low Temp. Phys.* **122** 265 (2001)
26. T Kumada, M Sakakibara, T Nagasaka, H Fukuta, J Kumagai, T Miyazaki *J. Chem. Phys.* **116** 1109 (2002)
27. T Kumada, K Komagauchi, Y Aratono, T Miyazaki *Chem. Phys. Lett.* **261** 463 (1996)
28. T Miyazaki, N Iwata, K Fueki, H Hase *J. Phys. Chem.* **94** 1702 (1990)
29. T Miyazaki *Chem. Phys. Lett.* **176** 99 (1991)
30. T Kumada, N Kitagawa, T Noda, J Kumagai, Y Aratono, T Miyazaki *Chem. Phys. Lett.* **288** 755 (1998)
31. T Kumada, T Noda, J Kumagai, Y Aratono, T Miyazaki *J. Chem. Phys.* **111** 10974 (1999)
32. J Kumagai, T Noda, T Miyazaki *Chem. Phys. Lett.* **321** 8 (2000)
33. *Atom Tunnelling Phenomena in Physics, Chemistry and Biology* (Ed. T Miyazaki) (Berlin: Springer, 2004)
34. G K Ivanov, M A Kozhushner, L I Trakhtenberg *J. Chem. Phys.* **113** 1992 (2000)
35. J Z H Zhang, W H Miller *J. Chem. Phys.* **91** 1528 (1989)
36. E B Gordon, L P Mezhov-Deglin, O F Pugachev *Pisma Zh. Exp. Teor. Fiz.* **19** 103 (1974) [b]
37. E B Gordon, V V Khmelenko, E A Popov, A A Pelmenev, O F Pugachev *Chem. Phys. Lett.* **155** 301 (1989)
38. V Kiryukhin, B Keimer, R E Boltnev, V V Khmelenko, E B Gordon *Phys. Rev. Lett.* **79** 1774 (1997)
39. S I Kiselev, V V Khmelenko, D M Lee, V Kiryukhin, R E Boltnev, E B Gordon, B Keimer *Phys. Rev. B* **65** 024517 (2002)
40. E B Gordon *Dokl. Akad. Nauk* **378** 156 (2001) [d]
41. R W H Webeler *J. Chem. Phys.* **64** 2253 (1976)
42. J Ahokas, J Jarvinen, V V Khmelenko, D M Lee, S Vasiliev *Phys. Rev. Lett.* **97** 095301 (2006)
43. S Vasiliev, J Jarvinen, E Tjukanov, A Kharitonov, S Jaakola *Rev. Sci. Instrum.* **75** 94 (2004)
44. S I Kiselev, V V Khmelenko, E P Bernard, D M Lee *Fiz. Nizk. Temp.* **29** 505 (2003) [c]
45. E P Bernard, V V Khmelenko, E Vehmanen, P P Borbat, J H Freed, D M Lee *AIP Conference Proceedings 850: The 24th International Conference on Low Temperature Physics, Orlando, FL, 2005* p. 1659
46. W E Blumberg, W B Mims, D Zuckerman *Rev. Sci. Instrum.* **44** 546 (1973)
47. A V Astashkin, V V Kozlyuk, A M Raitsimring *J. Magn. Reson.* **145** 357 (2000)
48. S I Kiselev, V V Khmelenko, C Y Lee, D M Lee *J. Low Temp. Phys.* **128** 37 (2002)
49. S I Kiselev, V V Khmelenko, D M Lee *Phys. Rev. Lett.* **89** 175301 (2002)
50. V V Khmelenko, S I Kiselev, D M Lee, C Y Lee *Phys. Scr.* **T102** 118 (2002)
51. E P Bernard, R E Boltnev, V V Khmelenko, D M Lee *J. Low Temp. Phys.* **138** 829 (2005)
52. G T Trammell, H Zeldes, R Livingston *Phys. Rev.* **110** 630 (1958)
53. T Kumada *J. Chem. Phys.* **124** 094504 (2006)
54. E P Bernard, V V Khmelenko, E Vehmanen, P P Borbat, J H Freed, D M Lee *AIP Conference Proceedings 850: The 24th International Conference on Low Temperature Physics, Orlando, FL, 2005* p. 372
55. W B Mims, J Peisach, J L Davis *J. Chem. Phys.* **66** 5536 (1977)
56. M Iwasaki, K Toriyama, K Nunome *J. Chem. Phys.* **86** 5971 (1987)
57. A Ponti *J. Magn. Reson.* **127** 87 (1997)
58. E B Gordon *Fiz. Nizk. Temp.* **30** 756 (2004) [c]
59. V V Khmelenko, E P Bernard, E Vehmanen, D M Lee *AIP Conference Proceedings 850: The 24th International Conference on Low Temperature Physics, Orlando, FL, 2005* p. 376
60. J Järvinen, J Ahokas, S Jaakkola, S Vasilyev *Phys. Rev. A* **72** 052713 (2005)
61. Y M Xiao, S Buchman, L Pollack, D Kleppner, T J Greytak *Phys. Rev. B* **48** 15744 (1993)
62. S N Foner, E L Cochran, V A Bowers, C K Jen *J. Chem. Phys.* **32** 963 (1960)
63. Yu Kagan, A J Leggett *Quantum Tunnelling in Condensed Media* (Amsterdam: North-Holland, 1992)
64. D O Edwards, A S McWilliams, J G Daunt *Phys. Rev. Lett.* **9** 195 (1962)
65. V Maidanov, A Ganshin, V Grigor'ev, A Penzev, E Rudavskii, A Rybalko, Ye Syrnikov *J. Low Temp. Phys.* **126** 133 (2002)
66. H Meyer *Can. J. Phys.* **65** 1453 (1987)
67. H Meyer *Fiz. Nizk. Temp.* **24** 507 (1998) [c]
68. D I Pushkarev *Centr. Eur. J. Phys.* **2** 420 (2004)

[a] — *J. Exp. Theor. Phys. (Engl. Transl.)*
[b] — *J. Exp. Theor. Phys. Lett. (Engl. Transl.)*
[c] — *Low Temp. Phys. (Engl. Transl.)*
[d] — *Dokl. Phys. Chem. (Engl. Transl.)*